Parametric Analysis for Robust Force/Torque Tracking Control of a Virtual Stiffness-Damping System in Airfoil Aeroelasticity Testing

Difan Tang, Lei Chen, Zhao Feng Tian and Eric Hu

Abstract— **The force/torque tracking control of a virtual stiffness-damping system (VSDS) for airfoil aeroelasticity testing is studied in this paper. Existing test-beds rely on elastic elements or structures to set airfoil elasticity in tests, which can be costly and inconvenient in cases of frequent stiffness adjustment across a wide range. A possible alternative is the VSDS that utilizes electric drives to simulate the effects of structural elasticity and damping, as seen in marine and biomechanics engineering. However, the potential VSDS for airfoil aeroelasticity testing is more prone to transmission power-loss caused by generally unknown inputs including frictions as well as other un-modeled dynamics and disturbances, due to different operation principle and conditions compared with other existing VSDSs. This is a critical problem that can result in inaccurate virtual stiffness and damping. In this paper we tackle this problem by treating power loss as an unknown input and employing the linear-quadratic-Gaussian (LQG) tracking control enhanced by unknown-input estimation (UIE). A systematic procedure based on numerical study is proposed to investigate the effects of UIE-related parameters on system sensitivity and stability robustness. To confront uncertainties in parametric analysis, a stability robustness index is proposed. Findings from the proposed parametric analysis not only assist effective controller design but also correct and supplement the existing knowledge in literature. Wind-tunnel experiments were conducted with comparisons drawn between standard LQG tracking control and the UIE-LQG scheme, and satisfactory performance of the VSDS under the systematically synthesized UIE-LQG control was confirmed.**

I. Introduction

Airfoil aeroelasticity studies the interaction between aerodynamic loads and airfoil structures, the typical dynamic instability of which, generally known as flutter, can be destructive to airfoils [1]. For safety concerns and more efficient flight, numerous test-beds have been built for investigating airfoil flutter and suppression [2]–[5]. The usefulness of these test-beds has nonetheless been limited by the inconvenience in circumstances where frequent change of stiffness and damping properties across a wide range is desired, due to the involvement of physical elastic elements for airfoil stiffness setting. A more efficient low-cost alternative can be the virtual stiffness-damping system (VSDS) that uses electric motors to simulate the effects of springs and dampers, as seen in marine engineering [6]–[11] and biomechanics applications involving virtual reality and augmented reality such as digital twin technology [12].

The existing VSDSs are of one degree-of-freedom (DOF) whereas aeroelastic behaviors consist of a minimum of two DOFs. Extending the concept of 1-DOF VSDS to 2 DOFs needs to address the dynamics coupling between each DOF for proper force/torque control. The 2-DOF aeroelastic dynamics are coupled with respect to the displacement of each DOF, and this makes position tracking with force measurement feedback as in [6]–[8] difficult. Instead, using the computed-torque approach based on experimentally identified formula without force feedback [9]–[11] can bypass the dynamics coupling in displacements, which however, necessitates extensive system identification and calibration procedures. In the interests of enhanced robustness and ease of maintenance with simplified system identification and calibration procedures, the 2-DOF VSDS for airfoil aeroelasticity testing can be based on direct force/torque control with force/torque measurement feedback, which is different from that of [6]–[11]. Although similar operation principle can be found in biomechanics applications [12], direct implementation in airfoil aeroelasticity testing is difficult due to application purposes, requirements, and operation conditions being much different.

Because of the different operation principle compared with that of [6]–[11], the 2-DOF VSDS for airfoil aeroelasticity testing is more prone to power loss caused by transmission frictions as well as other un-modeled dynamics and disturbances (collectively categorized as 'unknown inputs'). The power loss needs to be properly compensated for accurate force/torque output according to desired stiffness and damping, and this raises high requirements to controller robustness. Improving the robustness of a controller via conventional approaches [13] is effective in most situations (e.g., the existing VSDSs) but inadequate for the 2-DOF VSDS in airfoil aeroelasticity testing (to be further detailed in this paper). Further improvement is made possible via techniques based on unknown-input estimation (UIE) and cancellation widely studied and applied in industrial applications, featuring enhanced tolerance to un-modeled dynamics and exogenous disturbances [14]–[21]. Therefore, in this study we investigate the linear-quadratic-Gaussian (LQG) tracking control integrated with UIE as in [19] to tackle the problem of transmission power-loss involved in the force/torque tracking of the 2-DOF VSDS for airfoil aeroelasticity testing.

Although brief guidelines for UIE synthesis are available in literature, there is lack of understanding on how different selection of UIE parameters affect system sensitivity and stability robustness to unknown inputs, which are crucial to the estimation and compensation of transmission power-loss. Given the numerous design parameters and the 2 DOFs

Difan Tang, Lei Chen, Zhao F. Tian, and Eric Hu are with School of Mechanical Engineering, University of Adelaide, SA 5005, Australia lei.chen@adelaide.edu.au

involved, conventional trial-and-error approach is deemed inadequate to yield satisfactory control. Accordingly, as major technical contributions of this paper:

1) A systematic procedure is proposed for numerical studies investigating the influence of UIE parameters on system sensitivity and stability robustness;
2) To confront uncertainties encountered in controller parametric analysis, a stability robustness index is proposed;
3) New findings are obtained from the proposed parametric analysis which correct and supplement the existing knowledge in literature. New guidelines for UIE synthesis are given, contributing new understanding and knowledge.
4) Experimental validation was performed in a wind tunnel on a VSDS prototype for airfoil aeroelasticity testing to confirm the effectiveness and validity of the UIE-LQG method and the proposed parametric analysis. To the best of our knowledge, the systematically synthesized robust force/torque tracking control enables the first successful VSDS implementation for airfoil aeroelasticity testing.

II. Aeroelastic Model

Aeroelastic flutter, viewed from a rigid airfoil section attached to elastic elements, can be described by oscillations in plunge and pitch degree-of-freedom (DOF). The corresponding 2-DOF aeroelastic system is illustrated in Fig. 1 and in this study we consider a subsonic-regime model [4] with an equation of motion taking the form of

$$\boldsymbol{m}\ddot{\boldsymbol{q}} + \boldsymbol{c}\dot{\boldsymbol{q}} + \boldsymbol{k}\boldsymbol{q} + \boldsymbol{F}_c = \boldsymbol{F}_{aero}, \tag{1}$$

with

$$\boldsymbol{q} = \begin{bmatrix} h \\ \alpha \end{bmatrix}, \quad \boldsymbol{F}_{aero} = \begin{bmatrix} -F_l \\ F_m \end{bmatrix}, \quad \boldsymbol{F}_c = \begin{bmatrix} -m_w \dot{\alpha}^2 r_\alpha b \sin\alpha \\ 0 \end{bmatrix},$$

$$\boldsymbol{m} = \begin{bmatrix} m_w & m_w r_\alpha b \cos\alpha \\ m_w r_\alpha b \cos\alpha & I_\alpha \end{bmatrix},$$

$$\boldsymbol{c} = \begin{bmatrix} c_h & 0 \\ 0 & c_\alpha \end{bmatrix}, \quad \boldsymbol{k} = \begin{bmatrix} k_h & 0 \\ 0 & k_\alpha \end{bmatrix},$$

$$F_l = \rho U_\infty^2 b^2 l_s C_{l\alpha} \left[\alpha + \dot{h}/U_\infty + (0.5 - a)\, b\dot{\alpha}/U_\infty \right],$$

$$F_m = \rho U_\infty^2 b^3 l_s C_{m_{\alpha e}} \left[\alpha + \dot{h}/U_\infty + (0.5 - a)\, b\dot{\alpha}/U_\infty \right],$$

$$C_{l\alpha} = \partial C_l/\partial\alpha, \quad C_{m_{\alpha e}} = (0.5 + a)\, C_{l\alpha} + 2\partial C_m/\partial\alpha,$$

where geometry and force related parameters and variables are defined in Fig. 1, and other terms are defined as

m_w:	airfoil mass;
I_α:	airfoil rotational inertia about its elastic axis;
k_h, k_α:	Stiffness coefficients of plunge and pitch DOFs;
c_h, c_α:	Damping coefficients of plunge and pitch DOFs;
ρ:	air density;
l_s:	airfoil span;
C_l:	airfoil lift coefficient;
C_m:	airfoil moment coefficient at 1/4 chord;
U_∞:	airflow velocity.

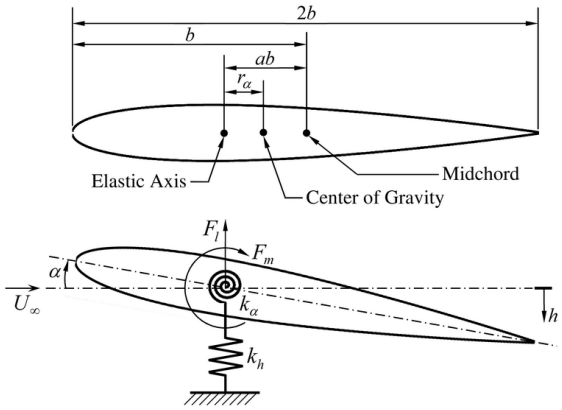

Fig. 1. 2-DOF aeroelastic system.

Denote the forces resulted from structural stiffness and damping by $\boldsymbol{F}_s$. Then according to (1), there is

$$\boldsymbol{F}_s(\boldsymbol{q}, \dot{\boldsymbol{q}}) = \boldsymbol{c}\dot{\boldsymbol{q}} + \boldsymbol{k}\boldsymbol{q}. \tag{2}$$

The compound force $\boldsymbol{F}_s(\boldsymbol{q}, \dot{\boldsymbol{q}})$, in the absence of physical springs and dampers, can be generated by a virtual stiffness-damping system described next.

III. Virtual stiffness-damping System

A. Mechanical Design

The mechanical design of the virtual stiffness-damping system (VSDS) considered in this study is given in Fig. 2. The pitching shafts of the VSDS and the airfoil are connected by a 6-axis force/torque transducer (ATI® Mini40) for measuring the 'elastic and damping' forces (generated by the VSDS) exerted on the airfoil. The plunge and pitch DOFs are each driven by an electric motor with an embedded encoder for position feedback. Rotation is converted to linear displacement for the plunge DOF via synchronous-belt transmission.

B. Dynamics

Although the dynamics of plunge and pitch DOFs are coupled with respect to plunge and pitch displacements according to (1), the two DOFs are independent of each other in terms of $\boldsymbol{F}_s$. For controller analysis and synthesis, dynamics from motor control input to measured force/torque output of both DOFs of the VSDS prototype were obtained through black-box system identification. Estimated models are linear time-invariant and in state-space form as

$$\begin{cases} \dot{\boldsymbol{x}} = \boldsymbol{A}_s\boldsymbol{x} + \boldsymbol{B}_s\boldsymbol{u}, \\ \bar{\boldsymbol{F}}_s = \boldsymbol{C}_s\boldsymbol{x} + \boldsymbol{D}_s\boldsymbol{u}, \end{cases} \tag{3}$$

where $\boldsymbol{x} \in \mathbb{R}^{n_x}$ contains n_x system states; $\bar{\boldsymbol{F}}_s \in \mathbb{R}^{n_F}$ contains n_F measured outputs; $\boldsymbol{u} \in \mathbb{R}^{n_u}$ contains n_u control inputs; $\boldsymbol{A}_s \in \mathbb{R}^{n_x \times n_x}$, $\boldsymbol{B}_s \in \mathbb{R}^{n_x \times n_u}$, $\boldsymbol{C}_s \in \mathbb{R}^{n_F \times n_x}$, and $\boldsymbol{D}_s \in \mathbb{R}^{n_F \times n_u}$ are system matrices.

Power loss is partly captured by the experimentally identified models (Table. I) but modeling errors and other types of disturbances (together defined as 'unknown inputs') can still

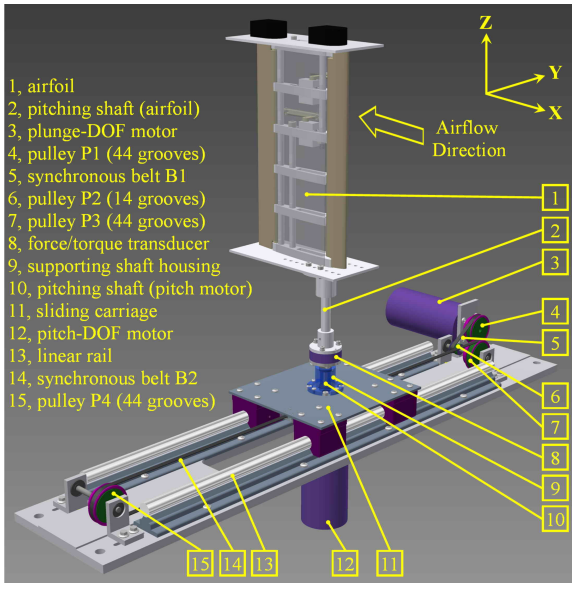

Fig. 2. Overview of the VSDS for airfoil aeroelasticity testing.

TABLE I
VSDS PROTOTYPE DYNAMICS

DOF	Matrices of System Dynamics				Fit (%)
	$\boldsymbol{A}_s$	$\boldsymbol{B}_s$	$\boldsymbol{C}_s$	$\boldsymbol{D}_s$	
Plunge	$\begin{bmatrix} -8.791 & 364 \\ -273.8 & -165.9 \end{bmatrix}$	$\begin{bmatrix} 45.5 \\ 29.19 \end{bmatrix}$	$\begin{bmatrix} 25.53 \\ 3.903 \end{bmatrix}^{\mathrm{T}}$	0	93.88
Pitch	$\begin{bmatrix} 18.67 & -464 \\ 429.1 & -716.3 \end{bmatrix}$	$\begin{bmatrix} 5823 \\ 7501 \end{bmatrix}$	$\begin{bmatrix} 0.4412 \\ -0.0669 \end{bmatrix}^{\mathrm{T}}$	0	94.04

have significant impact on the accuracy of virtual stiffness and damping simulated by electric drives. To tackle this, we rewrite (3) as

$$\begin{cases} \dot{\boldsymbol{x}} = \boldsymbol{A}_s\boldsymbol{x} + \boldsymbol{B}_s\boldsymbol{u} + \boldsymbol{B}_d\boldsymbol{d}, \\ \bar{\boldsymbol{F}}_s = \boldsymbol{C}_s\boldsymbol{x}, \end{cases} \tag{4}$$

where $\boldsymbol{d} \in \mathbb{R}^{n_d}$ contains n_d unknown inputs perturbing the system; $\boldsymbol{B}_d \in \mathbb{R}^{n_x \times n_d}$ is the unknown-input distribution matrix.

Since the models in Table. I are controllable, observable, and on the imaginary axis there is no zeros, according to [22], an equivalent of $\boldsymbol{d}$ exists which enters the system via $\boldsymbol{B}_s$. Therefore, system (4) is equivalent to

$$\begin{cases} \dot{\boldsymbol{x}} = \boldsymbol{A}_s\boldsymbol{x} + \boldsymbol{B}_s\left(\boldsymbol{u} + \boldsymbol{d}_e\right), \\ \bar{\boldsymbol{F}}_s = \boldsymbol{C}_s\boldsymbol{x}, \end{cases} \tag{5}$$

where $\boldsymbol{d}_e \in \mathbb{R}^{n_u}$ contains the equivalent unknown inputs.

C. Force/Torque Tracking Controller

As discussed in Section II, the VSDS needs to generate $\boldsymbol{F}_s(\boldsymbol{q}, \dot{\boldsymbol{q}})$ in the absence of physical springs. Hence, it is a force/torque tracking problem, where the reference trajectories $\boldsymbol{F}_s(\boldsymbol{q}, \dot{\boldsymbol{q}})$ change in real time with respect to $\boldsymbol{q}$ and $\dot{\boldsymbol{q}}$ in accordance with (2). To deal with transmission power-loss, the linear-quadratic-Gaussian (LQG) tracking control

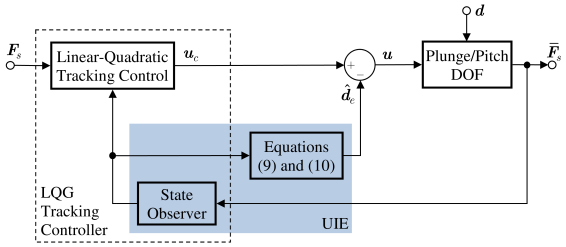

Fig. 3. Schematic diagram of the UIE-LQG controller.

enhanced by unknown-input estimation (UIE) as in [19] is employed for the VSDS prototype, given the existence of an equivalent system as in (5). The controller has a structure illustrated in Fig. 3, which consists of a standard LQG tracking component and a UIE add-on. The LQG control provides nominal force/torque tracking, while the UIE estimates and compensates transmission power-loss. Detailed composition of the controller, without distinguishing between specific DOFs, is given below in a general multiple-input multiple-output form.

The total control $\boldsymbol{u}$ is

$$\boldsymbol{u} = \boldsymbol{u}_c - \hat{\boldsymbol{d}}_e, \tag{6}$$

where $\boldsymbol{u}_c$ is from the LQG component for trajectory tracking, and $\hat{\boldsymbol{d}}_e$ is the estimated equivalent power loss.

The nominal control $\boldsymbol{u}_c$ takes the form of

$$\boldsymbol{u}_c = -\boldsymbol{K}_x\hat{\boldsymbol{x}} - \boldsymbol{K}_w\boldsymbol{x}_w + \boldsymbol{K}_f\boldsymbol{F}_s(\boldsymbol{q}, \dot{\boldsymbol{q}}), \tag{7}$$

with

$$\dot{\boldsymbol{x}}_w = \boldsymbol{F}_s(\boldsymbol{q}, \dot{\boldsymbol{q}}) - \bar{\boldsymbol{F}}_s = \boldsymbol{F}_s(\boldsymbol{q}, \dot{\boldsymbol{q}}) - \boldsymbol{C}_s\boldsymbol{x}, \tag{8}$$

where $\boldsymbol{K}_x \in \mathbb{R}^{n_u \times n_x}$, $\boldsymbol{K}_w \in \mathbb{R}^{n_u \times n_F}$, and $\boldsymbol{K}_f \in \mathbb{R}^{n_u \times n_F}$ are gains of the LQG tracking control which can be selected following standard LQG design procedures [23].

The power-loss estimation $\hat{\boldsymbol{d}}_e$ is obtained via

$$\hat{\boldsymbol{d}}_e = \hat{\boldsymbol{d}}_{ev} + \boldsymbol{K}_d\left(\bar{\boldsymbol{F}}_s - \hat{\bar{\boldsymbol{F}}}_s\right), \tag{9}$$

with

$$\begin{cases} \dot{\boldsymbol{x}}_f = \boldsymbol{A}_f\boldsymbol{x}_f + \boldsymbol{B}_f\hat{\boldsymbol{d}}_e, \\ \hat{\boldsymbol{d}}_{ev} = \boldsymbol{C}_f\boldsymbol{x}_f, \end{cases} \tag{10}$$

and

$$\begin{cases} \dot{\hat{\boldsymbol{x}}} = \boldsymbol{A}_s\hat{\boldsymbol{x}} + \boldsymbol{B}_s\boldsymbol{u}_c + \boldsymbol{L}\left(\bar{\boldsymbol{F}}_s - \hat{\bar{\boldsymbol{F}}}_s\right), \\ \hat{\bar{\boldsymbol{F}}}_s = \boldsymbol{C}_s\hat{\boldsymbol{x}}, \end{cases} \tag{11}$$

where $\boldsymbol{K}_d \in \mathbb{R}^{n_u \times n_F}$ is the UIE gain; $\hat{\bar{\boldsymbol{F}}}_s$ contains estimated system outputs; $\boldsymbol{A}_f \in \mathbb{R}^{n_f \times n_f}$, $\boldsymbol{B}_f \in \mathbb{R}^{n_f \times 1}$, and $\boldsymbol{C}_f \in \mathbb{R}^{1 \times n_f}$ are matrices of a low-pass-filter-characterized subsystem $(\boldsymbol{A}_f, \boldsymbol{B}_f, \boldsymbol{C}_f)$ with n_f states; $\boldsymbol{L} \in \mathbb{R}^{n_x \times 1}$ is the state observer gain; $\hat{\boldsymbol{x}}$ contains estimated system states.

The UIE gain $\boldsymbol{K}_d$ can be calculated via linear-quadratic optimization based on the dynamics of states estimation:

$$\begin{cases} \dot{\boldsymbol{e}}_x = (\boldsymbol{A}_s - \boldsymbol{L}\boldsymbol{C}_s)\boldsymbol{e}_x - \boldsymbol{B}_s\boldsymbol{K}_d\boldsymbol{C}_s\boldsymbol{e}_x + \boldsymbol{\xi}', \\ \boldsymbol{e}_F = \boldsymbol{C}_s\boldsymbol{e}_x, \end{cases} \tag{12}$$

where $\boldsymbol{e}_{_F} = \bar{\boldsymbol{F}}_s - \hat{\bar{\boldsymbol{F}}}_s$ and $\boldsymbol{\xi}^{'} = \boldsymbol{d}_e - \hat{\boldsymbol{d}}_{ev}$.

Upon $\boldsymbol{\xi}^{'} \approx 0$, we have

$$\dot{\boldsymbol{e}}_x = (\boldsymbol{A}_s - \boldsymbol{L}\boldsymbol{C}_s - \boldsymbol{B}_s\boldsymbol{K}_d\boldsymbol{C}_s)\boldsymbol{e}_x. \tag{13}$$

For observable systems, the pair $(\boldsymbol{A}_s - \boldsymbol{L}\boldsymbol{C}_s,\ \boldsymbol{C}_s)$ is observable. Under duality, there exists $\boldsymbol{K}_v = (\boldsymbol{B}_s\boldsymbol{K}_d)^{\mathrm{T}}$ that minimizes

$$J_d = \int_0^\infty \left\{\boldsymbol{e}_x^{\mathrm{T}}\boldsymbol{Q}_d\boldsymbol{e}_x + \boldsymbol{e}_{dv}^{\mathrm{T}}\boldsymbol{R}_d\boldsymbol{e}_{dv}\right\} dt, \tag{14}$$

with $\boldsymbol{Q}_d \in \mathbb{R}^{n_x \times n_x}$ and $\boldsymbol{R}_d \in \mathbb{R}^{n_F \times n_F}$ being symmetric positive-definite weighting matrices.

Therefore,

$$\boldsymbol{K}_d = {\boldsymbol{B}_s}^{\dagger}\boldsymbol{K}_v^{\mathrm{T}}, \tag{15}$$

with ${\boldsymbol{B}_s}^{\dagger}$ being the Moore-Penrose pseudo inverse of $\boldsymbol{B}_s$.

As can be seen from (9) to (11), the UIE gain $\boldsymbol{K}_d$, the low-pass-filter-characterized subsystem $(\boldsymbol{A}_f, \boldsymbol{B}_f, \boldsymbol{C}_f)$, and the state observer gain $\boldsymbol{L}$ are major design parameters related to the UIE component.

IV. Controller Analysis

System sensitivity and stability robustness, being crucial to estimation and compensation of transmission power-loss, are major concerns in controller synthesis for the VSDS prototype in airfoil aeroelasticity testing. Although brief guidelines for selecting UIE-related parameters are provided in literature, there is lack of understanding on the influence of these design parameters on system sensitivity and stability robustness. As a major contribution, numerical studies are presented in this section, delivering parametric analysis of these design variables in terms of their respective influence on system sensitivity and stability robustness. Findings from the analysis not only assist effective VSDS controller design but also correct the existing knowledge in literature, with new guidelines for synthesizing the UIE component given.

Given the single-input single-output (SISO) feature of VSDS plunge/pitch-DOF dynamics (Table. I), the following analysis is performed on an SISO basis.

In frequency domain, equation (5) takes the form of

$$\bar{F}_s(s) = P_n(s)\left[u(s) + d_e(s)\right], \tag{16}$$

where $P_n(s)$ is the nominal model of the VSDS plunge/pitch DOF.

In this SISO case, any individual tracking trajectory from the set $\boldsymbol{F}_s(\boldsymbol{q}, \dot{\boldsymbol{q}})$ is denoted by $F_s(s) \subseteq \boldsymbol{F}_s$ for convenience in notation. With $G_w(s)$ denoting the transfer function of the integral action, equation (7) can be transformed into

$$u_c(s) = -\boldsymbol{K}_x\hat{\boldsymbol{x}}(s) - K_w x_w(s) + K_f F_s(s), \tag{17}$$

with $x_w(s) = G_w(s)\left[F_s(s) - \bar{F}_s(s)\right]$.

By using (17) in (11), and with $F_s(s) = 0$, there is

$$\hat{\boldsymbol{x}}(s) = \boldsymbol{G}_{yx}(s)\bar{F}_s(s), \tag{18}$$

with

$$\boldsymbol{G}_{yx}(s) = \left(s\boldsymbol{I}_{n_x} - \boldsymbol{A} + \boldsymbol{B}\boldsymbol{K}_x + \boldsymbol{L}\boldsymbol{C}\right)^{-1}\left[\boldsymbol{B}K_wG_w(s) + \boldsymbol{L}\right].$$

From (9) and (10), we have

$$\hat{d}_{ev}(s) = G_f(s)\hat{d}_e(s), \tag{19}$$

$$\hat{d}_e(s) = G_{yd}(s)\left[\bar{F}_s(s) - \hat{\bar{F}}_s(s)\right], \tag{20}$$

where

$$G_f(s) = \boldsymbol{C}_f(s\boldsymbol{I}_{n_f} - \boldsymbol{A}_f)^{-1}\boldsymbol{B}_f\hat{d}_e(s),$$

$$G_{yd}(s) = [1 - G_f(s)]^{-1}K_d.$$

Based on (6), (16) to (18), and (20), we reach

$$\bar{F}_s(s) = P_n(s)[1 + H_s(s)P_n(s)]^{-1}d_e(s), \tag{21}$$

where

$$H_s(s) = \boldsymbol{K}_x\boldsymbol{G}_{yx}(s) - K_wG_w(s) + G_{yd}(s)\left[1 - \boldsymbol{C}\boldsymbol{G}_{yx}(s)\right].$$

Thus, the system sensitivity to unknown inputs (simply referred to as 'sensitivity' in short hereinafter) is

$$S_s(j\omega) = \frac{1}{1 + H_s(j\omega)P_n(j\omega)}, \quad \forall\omega \in [0, +\infty). \tag{22}$$

To allow evaluating sensitivity against different values of the cutoff frequency ω_c of subsystem $(\boldsymbol{A}_f, \boldsymbol{B}_f, \boldsymbol{C}_f)$, the magnitude of sensitivity with regard to inputs of a certain natural frequency (i.e., $|S_s(j\omega_d)|$) is considered. In the analysis, $\omega_d = 5$ rad/s is considered, according to the spectrum characteristics of system identification data.

In the presence of uncertainties $\delta(j\omega), \forall\omega \in [0, +\infty)$, closed-loop stability is guaranteed if

$$|\delta(j\omega)| < \left|1 + \frac{1}{H_s(j\omega)P_n(j\omega)}\right|,\ \forall\omega \in [0, +\infty). \tag{23}$$

As it is common that there is little or no priori knowledge about $\delta(j\omega)$, a conservative choice is to assume $\delta(j\omega) = 1, \forall\omega \in [0, +\infty)$. On this basis, the following stability robustness index (SRI) is proposed:

$$\text{SRI} = \min\left|1 + \frac{1}{H_s(j\omega)P_n(j\omega)}\right| - 1,\ \forall\omega \in [0, +\infty). \tag{24}$$

It is worth noting that due to the conservative assumption of $\delta(j\omega)$, a negative SRI is not necessarily a sign of instability. Instead, SRI gives a relative measure on stability robustness. That is, a larger SRI suggests better stability robustness.

To investigate the effects of using a low-pass filter (LPF) of different orders for the subsystem $(\boldsymbol{A}_f, \boldsymbol{B}_f, \boldsymbol{C}_f)$, the following generalized formulation $G_f(s)$ is considered:

$$G_f(s) = \frac{\sum_{i=0}^{p} a_{mi}(\tau s)^i}{(\tau s + 1)^m}, \tag{25}$$

where m is the denominator order and p is the numerator order; $a_{mi} = \frac{m!}{(m-i)!i!}$ is the i^{th} coefficient of the numerator polynomial; τ is the time constant.

Since the closed-loop system is unstable if $p \geq 1$, the analysis herein only considers cases where $m \geq 1$ and $p = 0$. This yields LPFs with a unity passband gain.

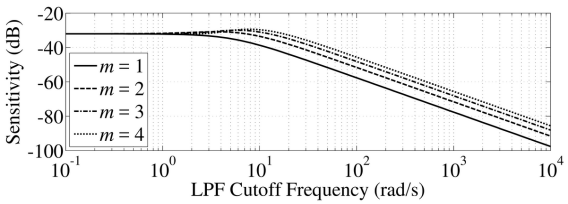

Fig. 4. Sensitivity at $\omega_d = 5$ rad/s against LPF cutoff frequency.

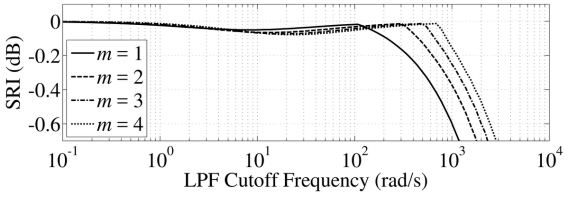

Fig. 5. Stability robustness index (SRI) against LPF cutoff frequency.

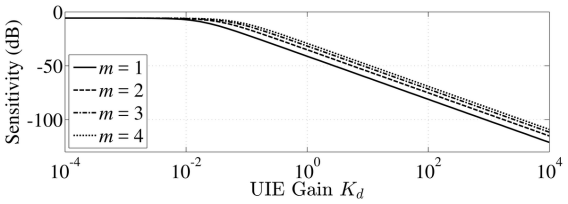

Fig. 6. Sensitivity at $\omega_d = 5$ rad/s against UIE gain.

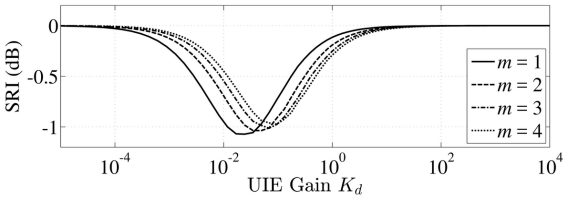

Fig. 7. Stability robustness index (SRI) against UIE gain.

Only the plunge-DOF dynamics of the VSDS prototype are used throughout the analysis, given similarity between both DOFs. Parameters of the standard LQG tracking control used in the analysis were fine-tuned in experiment to achieve as good tracking as possible with no overshoots and instability (caused by large gains), which are $\boldsymbol{K}_x = [6.27,\ 3.98]$, $K_w = -3.16$, and $K_f = 0.4$. These LQG parameters are exclusive to the UIE and are kept unchanged throughout the analysis while the UIE-related parameters are varied across regions of interest for investigation.

A. Low-Pass Filter Cutoff Frequency

In this analysis, the UIE component takes parameters of $\boldsymbol{L} = [9.49,\ 1.07]^{\mathrm{T}}$, $K_d = 6.64$, and $1 \leq m \leq 4,\ \forall m \in \mathbb{Z}$, with the LPF cutoff frequency ω_c being varied. Fig. 4 shows that sensitivity decreases with increased ω_c, when ω_c is times higher than ω_d. A first-order LPF requires the least gap between ω_d and ω_c to achieve useful sensitivity, while a fourth-order LPF introduces a mild peak in sensitivity, and ω_c needs to be 3 to 4 times higher than ω_d for reduced sensitivity. In Fig. 5, similar stability robustness can be observed among the four filters for $\omega_c < 10^2$ rad/s, all showing relatively good stability robustness. But differences start to grow for $\omega_c > 10^2$ rad/s, where the LPF of first-order is more sensitive to the increase of ω_c, having an earlier drop of stability robustness compared with LPFs of higher orders. Figs. 4 and 5 indicate that a first-order LPF can be a preferred choice from the sensitivity perspective, and is most suitable for low-frequency uncertainties in the interests of stability robustness. Figs. 4 and 5 also recommend that $\omega_c = 100$ rad/s is a relatively better choice that balances sensitivity and stability robustness. Therefore, $\omega_c = 100$ rad/s is used in the subsequent analysis.

B. Unknown-Input Estimation Gain

To study the effect of the UIE gain, K_d is considered as a variable while other parameters are set as $\boldsymbol{L} = [9.49,\ 1.07]^{\mathrm{T}}$, $\omega_c = 100$ rad/s, and $1 \leq m \leq 4,\ \forall m \in \mathbb{Z}$. It is straightforward to see from Fig. 6 that larger K_d contributes to smaller sensitivity, delivering better rejection of unknown inputs. However, a dip can been seen on each of the SRI curves in Fig. 7, indicating a weak stability robustness region, which should be avoided in design. K_d to the left of this potentially unstable region, being too small to make the UIE component effective, is not preferred. A larger K_d beyond the SRI dip can be considered in UIE design, as the stability robustness recovers to an acceptable level. Hence, Figs. 6 and 7 both support the choice for a larger K_d. LPFs of different orders do not have significant impact on K_d selection from the stability robustness perspective, although some shift of the dip on the SRI curve can be seen between LPFs of different orders. In the interests of better estimation and compensation of transmission power-loss, a first-order LPF can be considered for the relatively smaller sensitivity achieved with the same K_d. In [19], K_d is recommended only for fine tuning the UIE-LQG controller. The analysis in this paper implies that K_d can also be used as a primary design parameter instead of being merely designated for fine-tune. This finding corrects the guideline given in [19].

C. State Observer Gain

With UIE parameters $K_d = 6.64$, $\omega_c = 100$ rad/s, and $1 \leq m \leq 4,\ \forall m \in \mathbb{Z}$, the influence of $\boldsymbol{L}$ is evaluated. As can be seen in Fig. 8, the sensitivity remains at a low level and is insensitive to variation of $\boldsymbol{L}$ in the region where $\|\boldsymbol{L}\|_2 \in (0, 10^2]$, favored for estimation and compensation of transmission power-loss. $\boldsymbol{L}$ within this range is also acceptable in terms of stability robustness, as shown in Fig. 9. Continuously increasing $\boldsymbol{L}$ not only weakens unknown-inputs rejection capability with raised sensitivity (Fig. 8) but also can bring instability issues as indicated by the dip around $\|\boldsymbol{L}\|_2 \in [10^2, 10^5]$ (Fig. 9). Although stability robustness returns to an acceptable level with much larger $\boldsymbol{L}$, $\boldsymbol{L}$ within this high-value range is nevertheless undesired in consideration of weak rejection of unknown inputs and increased computation load. This finding corrects the guideline provided in [19] which does not restrict the

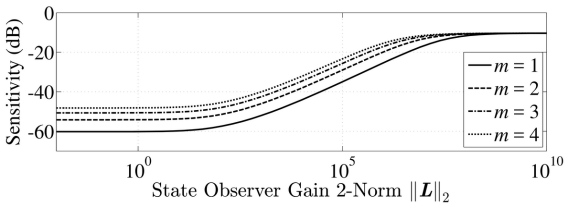

Fig. 8. Sensitivity at $\omega_d = 5$ rad/s against state observer gain.

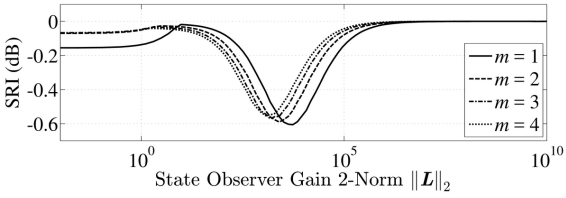

Fig. 9. Stability robustness index (SRI) against state observer gain.

design of $\boldsymbol{L}$. With regard to the effects of the LPF order, it is easy to see from Fig. 8 that a first-order LPF can be a better choice for relatively smaller sensitivity, with stability robustness property similar to LPFs of higher orders.

D. Controller Design Guidelines

Based on the proposed parametric analysis, new guidelines for synthesizing the UIE-LQG controller can be drawn:

- The LPF can take the first-order form, not only for less phase delay, but also for smaller sensitivity. There exists an upper limit for ω_c, beyond which stability robustness can drop dramatically;
- K_d is recommended to be as high as practically feasible (i.e., not incurring computation issues such as high computation load);
- Conventional LQG synthesis routine is not enough for selecting $\boldsymbol{L}$, which should be further evaluated by looking at both the robustness and sensitivity plots across a range of practically achievable $\boldsymbol{L}$ values.
- Specific values of ω_c, K_d, and $\boldsymbol{L}$ vary between applications, and can be determined using the proposed systematic procedure.

These new guidelines correct and supplement the brief instructions given in [19] and contribute new knowledge to the UIE-integrated control theory.

V. Experimental Validation

Validation of the controller design for the VSDS prototype was performed through wind-tunnel experiments with the setup shown in Fig. 10 and corresponding aeroelastic system parameters listed in Tables. II. The systematically synthesized parameters of the UIE-LQG controller are given in Table. III. Two cases are presented in this paper, the settings of which are summarized in Table. IV. In each case, comparisons are drawn between standard LQG tracking control (by disconnecting the UIE component) and the UIE-LQG control.

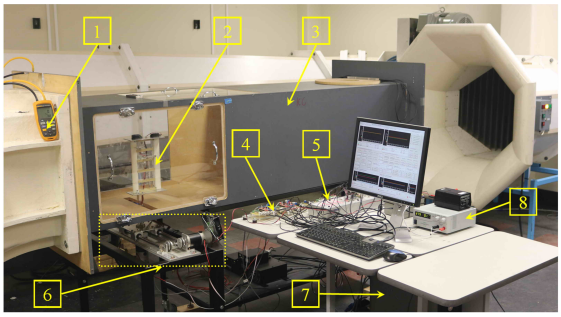

1 – pressure transducer connected to a Pitot tube; 2 – airfoil; 3 – wind tunnel test duct; 4 – I/O board; 5 – dSPACE® DS1104 R&D board; 6 – VSDS; 7 – PC; 8 – power.

Fig. 10. Wind-tunnel experiment setup.

TABLE II
Parameters of Wind-Tunnel Experiment Setup

Parameters	Values	Parameters	Values
a	-0.569	c_h, c_α, k_h, k_α	See Table. IV
b	0.075 m	m_α	0.851 kg
l_s	0.260 m	I_α	2.431×10^{-3} kg·m^2
r_α	0.033 m	$C_{l\alpha}$	6.573
ρ	1.225 kg/m^3	C_m	0

TABLE III
VSDS Controller Parameters

Parameters		Plunge DOF	Pitch DOF
Nominal Tracking	$\boldsymbol{K}_x$	$[6.27 \quad 3.98]$	$[4.39 \quad -0.74]$
	K_w	-3.16	-3.16
	K_f	0.4	10.08
Shared	$\boldsymbol{L}$	$[9.49 \quad 1.07]^{\mathrm{T}}$	$[7.33 \quad 2.19]^{\mathrm{T}}$
UIE	K_d	6.64	4.34
	$G_f(s)$	$\frac{1}{(0.01s+1)}$	$\frac{1}{(0.01s+1)}$

TABLE IV
Wind-Tunnel Experiment Scenarios

Case	Flutter Boundary	Airflow Speed	Stiffness & Damping
1	13.92 m/s	14.8 m/s	$k_h = 50 + 300h^2$ N/m $k_\alpha = 0.3 + 30\alpha^2$ Nm/rad $c_h = 14$ kg/s $c_\alpha = 0.042$ kg·m^2/s
2	16.02 m/s	16.8 m/s	k_h, k_α, c_h: same as Case 1 $k_\alpha = 0.77 + 30\alpha^2$ Nm/rad

Force/torque tracking performance of the VSDS prototype in the two test scenarios are shown in Figs. 11 to 14 and the resulted aeroelastic responses are plotted in Figs. 15 and 16. Significant differences between measurements and reference tracking trajectories can be observed in tests where standard LQG control was applied (Figs. 11 and 13). As a result, flutter failed to initiate under the LQG control as seen in Figs. 15 and 16, although the airflow speeds in tests were higher than corresponding flutter boundaries (i.e., the airflow velocity at and beyond which flutter occurs). In comparison, the measured plunge-DOF forces and pitch-DOF torques strictly follow the desired trajectories under the UIE-LQG

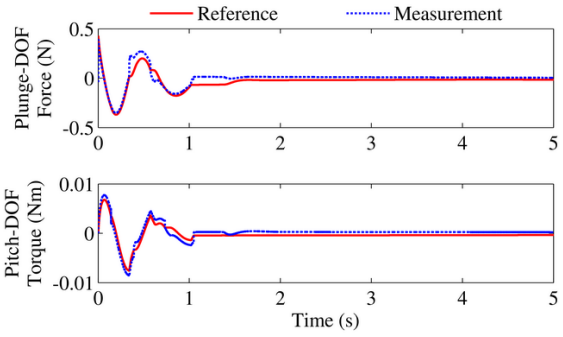

Fig. 11. VSDS force/torque under LQG control in Case 1 tests.

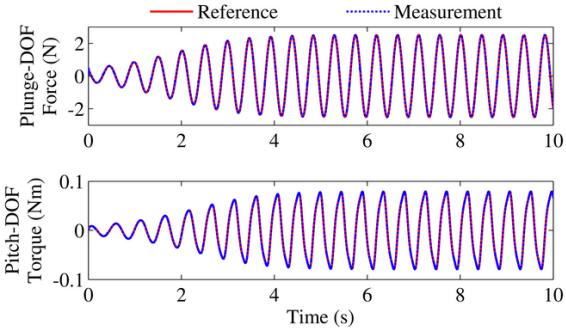

Fig. 12. VSDS force/torque under UIE-LQG control in Case 1 tests.

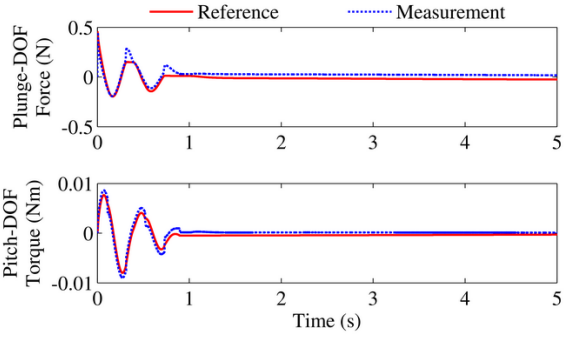

Fig. 13. VSDS force/torque under LQG control in Case 2 tests.

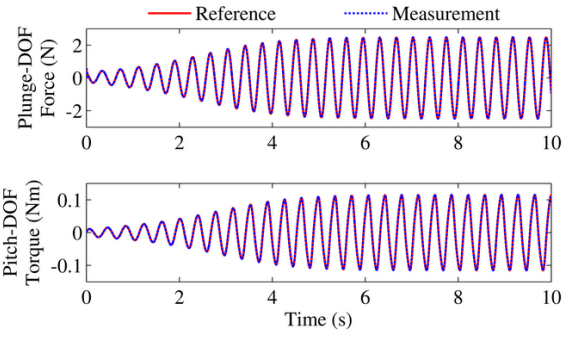

Fig. 14. VSDS force/torque under UIE-LQG control in Case 2 tests.

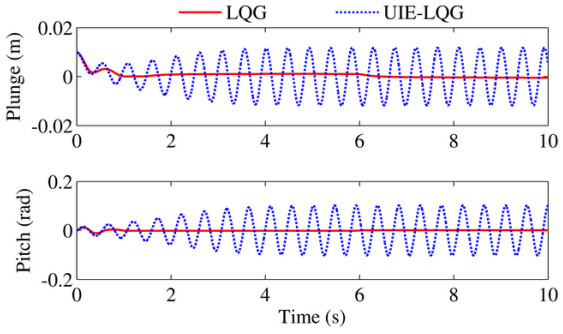

Fig. 15. Aeroelastic responses in Case 1 tests.

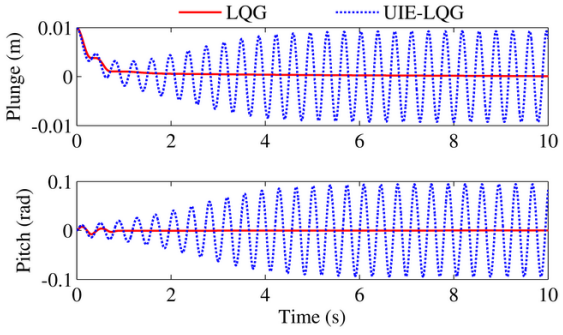

Fig. 16. Aeroelastic responses in Case 2 tests.

control, with tracking deviations barely identified (Figs. 12 and 14). This enabled successful initiation and development of flutter (Figs. 15 and 16). The experiment results indicate that: (1) The transmission power-loss, if not properly treated, have considerable impacts on VSDS performance in airfoil aeroelasticity testing; (2) Effective estimation and compensation of transmission power-loss requires enhanced controller robustness to unknown inputs; (3) The proposed systematic numerical procedure for controller parametric analysis is effective in assisting satisfactory controller synthesis that delivers superior force/torque tracking.

VI. Conclusion

As a first trial of the emerging digital twin technology in airfoil aeroelasticity testing, the VSDS considered in this study requires special attention to its force/torque tracking control in the presence of transmission power-loss, due to its different operation principle and conditions compared with existing VSDSs in other fields. The UIE-LQG tracking control was employed and the lack of understanding on the influence of UIE-related parameters on estimation and compensation of transmission power-loss has motivated the proposal of a systematic procedure for numerical studies on parametric analysis. In particular, a stability robustness index is proposed to address the uncertainties encountered in controller synthesis. The proposed parametric analysis delivers better understanding of the influence of UIE-related parameters on system sensitivity and stability robustness. Some new findings also correct the existing synthesis guidelines in literature, and new guidelines are given accordingly. The proposed parametric analysis and corresponding new findings together contribute new knowledge to the UIE-LQG control. Wind-tunnel experiments show that transmission

power-loss has significant impacts on VSDS performance in airfoil aeroelasticity testing if not properly treated. Experimental studies also confirm that the proposed systematic procedure for numerical studies on parametric analysis is effective in assisting satisfactory UIE-LQG design to provide superior force/torque tracking in the presence of transmission power-loss. To the best of our knowledge, the systematically synthesized robust force/torque tracking control enables the first successful VSDS implementation in airfoil aeroelasticity testing, contributing to a new development in the field of virtual reality and augmented reality.

REFERENCES

[1] Y. C. Fung, *An Introduction to the Theory of Aeroelasticity*, C. B. Millikan, Ed. NY: John Wiley & Sons, 1955.

[2] M. G. Farmer, "A two-degree-of-freedom flutter mount system with low damping for testing rigid wings at different angles of attack," National Aeronautics and Space Administration, Report NASA TM 83302, Apr. 1982.

[3] G. D. Miller, "Active flexible wing (AFW) technology," Air Force Wright Aeronautical Laboratories, Report AFWAL-TR-87-3096, Feb. 1988.

[4] T. O'Neil and T. W. Strganac, "Aeroelastic response of a rigid wing supported by nonlinear springs," *J. Aircr.*, vol. 35, no. 4, pp. 616–622, Jul-Aug 1998.

[5] E. L. Burnett, J. A. Beranek, B. T. Holm-Hansen, C. J. Atkinson, and P. M. Flick, "Design and flight test of active flutter suppression on the X-56A multi-utility technology test-bed aircraft," *Aeronaut. J.*, vol. 120, no. 1228, pp. 893–909, Jun. 2016.

[6] F. S. Hover, S. N. Miller, and M. S. Triantafyllou, "Vortex-induced vibration of marine cables: Experiments using force feedback," *J. Fluids Struct.*, vol. 11, no. 3, pp. 307–326, Apr. 1997.

[7] F. S. Hover, A. H. Techet, and M. S. Triantafyllou, "Forces on oscillating uniform and tapered cylinders in crossflow," *J. Fluid Mech.*, vol. 363, pp. 97–114, May 1998.

[8] J. F. Derakhshandeh, M. Arjomandi, B. S. Cazzolato, and B. Dally, "Harnessing hydro-kinetic energy from wake-induced vibration using virtual mass spring damper system," *Ocean Eng.*, vol. 108, pp. 115–128, Nov. 2015.

[9] J. H. Lee, N. Xiros, and M. M. Bernitsas, "Virtual damper-spring system for VIV experiments and hydrokinetic energy conversion," *Ocean Eng.*, vol. 38, no. 5-6, pp. 732–747, Apr. 2011.

[10] J. Lee and M. Bernitsas, "High-damping, high-reynolds VIV tests for energy harnessing using the VIVACE converter," *Ocean Eng.*, vol. 38, no. 16, pp. 1697–1712, 2011.

[11] H. Sun, E. S. Kim, M. P. Bernitsas, and M. M. Bernitsas, "Virtual spring-damping system for flow-induced motion experiments," *J. Offshore Mech. Arct.*, vol. 137, no. 6, Dec. 2015.

[12] A. Kelly, *Mobile Robotics: Mathematics, Models, and Methods*. New York, NY: Cambridge University Press, 2013.

[13] K. J. Åström and T. Hägglund, *Advanced PID Control*. Research Triangle Park, NC: Instrumentation, Systems, and Automation Society, 2006.

[14] J.-H. She, X. Xin, and Y. Pan, "Equivalent-input-disturbance approach — analysis and application to disturbance rejection in dual-stage feed drive control system," *IEEE-ASME Trans. Mech.*, vol. 16, no. 2, pp. 330–340, Apr. 2011.

[15] S.-H. Lee, H. J. Kang, and C. C. Chung, "Robust fast seek control of a servo track writer using a state space disturbance observer," *IEEE Trans. Contr. Syst. T.*, vol. 20, no. 2, pp. 346–355, Mar. 2012.

[16] K. Erenturk, "Fractional-order $PI^{\lambda}D^{\mu}$ and active disturbance rejection control of nonlinear two-mass drive system," *IEEE Trans. Ind. Electron.*, vol. 60, no. 9, pp. 3806–3813, Sept. 2013.

[17] S. Zheng, B. Han, and L. Guo, "Composite hierarchical antidisturbance control for magnetic bearing system subject to multiple external disturbances," *IEEE Trans. Ind. Electron.*, vol. 61, no. 12, pp. 7004–7012, Dec. 2014.

[18] X. Chang, Y. Li, W. Zhang, N. Wang, and W. Xue, "Active disturbance rejection control for a flywheel energy storage system," *IEEE Trans. Ind. Electron.*, vol. 62, no. 2, pp. 991–1001, Feb. 2015.

[19] D. Tang, L. Chen, E. Hu, and Z. F. Tian, "A novel actuator controller: Delivering a practical solution to realization of active-truss-based morphing wings," *IEEE Trans. Ind. Electron.*, vol. 63, no. 10, pp. 6226–6237, Oct. 2016.

[20] B. Ren, Q.-C. Zhong, and J. Dai, "Asymptotic reference tracking and disturbance rejection of UDE-based robust control," *IEEE Trans. Ind. Electron.*, vol. 64, no. 4, pp. 3166–3176, Apr. 2017.

[21] P. Yu, M. Wu, J. She, K.-Z. Liu, and Y. Nakanishi, "An improved equivalent-input-disturbance approach for repetitive control system with state delay and disturbance," *IEEE Trans. Ind. Electron.*, vol. 65, no. 1, pp. 521–531, Jan. 2018.

[22] J.-H. She, M. Fang, Y. Ohyama, H. Hashimoto, and M. Wu, "Improving disturbance-rejection performance based on an equivalent-input-disturbance approach," *IEEE Trans. Ind. Electron.*, vol. 55, no. 1, pp. 380–389, Jan. 2008.

[23] B. D. O. Anderson and J. B. Moore, *Optimal Control: Linear Quadratic Methods*. Englewood Cliffs, NJ: Prentice-Hall, 1990.